Negative thermal expansion in supercooled tantala

F. Puosi*

Istituto Nazionale di Fisica Nucleare,

Largo B. Pontecorvo 3, I-56127 Pisa, Italy and

Dipartimento di Fisica "Enrico Fermi", Università di Pisa,

Largo B.Pontecorvo 3, I-56127 Pisa, Italy

F. Fidecaro, S. Capaccioli, D. Pisignano, and D. Leporini

Dipartimento di Fisica "Enrico Fermi", Università di Pisa,

Largo B.Pontecorvo 3, I-56127 Pisa, Italy and

Istituto Nazionale di Fisica Nucleare,

Largo B. Pontecorvo 3, I-56127 Pisa, Italy

Abstract

A density anomaly, i.e. a temperature region with negative thermal expansion (NTE) bounded by a density maximum and a density minimum at lower temperatures, is revealed and characterised in tantala for the first time by Molecular Dynamics simulations. The NTE region is evidenced in the metastable supercooled liquid and rather close to the glass transition. Since NTE is suppressed by poor structural equilibration, highlighting these phenomena is highly challenging due to the need for fulfilling competing constraints of slow cooling and avoidance of the crystallization. We find that the density anomaly is signalled by a decrease of the partial coordination numbers $n_{Ta,Ta}$ and $n_{O,O}$ when lowering the temperature. The NTE magnitude is comparable to the ones of both stable water and solid-state materials with giant NTE.

*Electronic address: francesco.puosi@pi.infn.it

I. INTRODUCTION

An isobaric density *maximum*, although well known in the case of water [1, 2], occurs in only a few liquids, e.g. heavy water (D_2O) [3], silica (SiO_2) [4], liquid Caesium (Cs) [5], Sulphur (S)[6] and Tellurium (Te) [7–9] where it is observed in equilibrium condition above their melting temperatures, or in liquid silicon (Si) where the maximum is in the supercooled regime [10]. Under isobaric conditions, below the temperature of maximum density, these liquids exhibit a region with negative thermal expansion (NTE), i.e. cooling the liquid causes it to expand. These unusual aspects of density behaviour are usually referred to as *density anomalies*.

Finding NTE materials is of technological importance and fundamental scientific interest. The discovery of NTE in Zirconium tungstate (ZrW_2O_8) in an extremely wide temperature range [11], attracted an ever growing interest in NTE materials [12–14]. The major motivation is the urgent demand of materials with vanishing or controlled thermal expansion in high-precision devices and instruments, e.g. fiber optics and mirror coatings, electronics, thermal actuators of microelectromechanical systems and tooth fillings. Novel routes for NTE compensation of ordinary, positive thermal expansion are under intense development [15].

Since for an ideal classical or quantum gas the linear thermal expansion α_L is positive, the microscopic origin of NTE lies in the interactions coupling the particles. Over the years, highly directional tetrahedral bonding interactions, like in water and silica, were intensively investigated. However, tetrahedrality is not a necessary condition for anomalous behavior. In fact, NTE is observed in both *p*-bonded liquids, like Tellurium and rich-Te alloys, exhibiting an octahedral environment [16] and even in *spherically symmetric* pair potentials [17, 18]. While these results widen the scenario of the microscopic mechanisms leading to NTE, the scaling of the anomalous thermodynamic properties of liquid water and tellurium on the same master curve suggests that even in the presence of deep structural differences, their anomalies have similar roots [19].

There is an intimate relation between NTE and *pairs* of density extrema. Thermodynamic consistency dictates that, if a given liquid exhibits a density extremum in its phase diagram, such a point cannot be isolated: a density extremum locus must necessarily exist. Leaving aside the possible termination of a density maxima locus at a stability limit, i.e. by crossing a spinodal curve, all the other thermodynamically-consistent scenarios imply the simultaneous existence of density *maxima* and *minima* [20, 21]. They correspond, respectively, to the highest and lowest possible temperatures at which a liquid can exhibit NTE [6, 22].

Experimental evidence of density *minima* in the liquid state is sparse. They were reported for equilibrium liquids, i.e. sulphur [6], As_2Te_3 [23], Ge/Se alloys [24], as well as for supercooled systems, i.e. nanoconfined water [25, 26], silica [4, 27] and Te [22]. Further evidence was provided by molecular-dynamics (MD) simulations in silica [28], Ge [29], the tetrahedral liquid BeF_2 [30, 31], water [32, 33] and monoatomic liquids with *spherical*, *pair* potentials including rather generic ramp potentials being both purely repulsive [17] and with both attractive and repulsive interactions (Jagla potential) [18].

The fact that the NTE region is often found in metastable supercooled liquids implies that it is potentially affected by the thermal history, i.e. the cooling rate driving the liquid to the glassy state. Provided that crystallization is avoided, slower cooling rates push the glass transition to lower temperatures, so that thermodynamics, and not off-equilibrium kinetics, are dominant in a wider temperature range [34]. Off-equilibrium overshadows and even suppresses both the extrema and the NTE region, as noted in SiO_2 by Brückner more than fifty years ago [4] and recently confirmed [28]. We argue that Brückner's conclusions have wider prospect and suggest a general search protocol of novel NTE materials based on proper structural equilibration and crystallization avoidance.

Here, we illustrate the protocol by presenting compelling evidence by MD simulations, that the oxide glassformer tantala (Ta_2O_5) exhibits *isotropic* NTE in a temperature region bounded by two density extrema both located in the metastable supercooled liquid. The NTE magnitude ($\alpha_L = -14$ ppm K^{-1}) is found to be one order of magnitude smaller than the one of liquid Tellurium but comparable to the ones of both stable water and solid-state materials with giant NTE. The structure of Ta_2O_5 is a network of Ta-centered polyhedra, mainly octahedra, with O atoms at their corners [35–37]. It is known that the crystal structures of many NTE materials are networks of both octahedra and tetrahedra [12, 13] and, for specific liquids, atoms have an octahedral environment [16]. Close examination of the structural changes occurring on cooling tantala across the NTE region reveals a reduction of the homologous first-neighbours, i.e. the coordination numbers $n_{Ta,Ta}$ and $n_{O,O}$. This mechanism leads to a volume increase. A decrease of the coordination number on cooling in the NTE region has been revealed in two supercooled atomic liquids, namely Te (octahedral), by both experiments [38] and simulations [39], and Ge (tetrahedral) by simulations [29]. Our results suggest that the family of M_2O_5 metal oxides adds to the NTE materials [13, 15, 34].

II. MODEL AND METHODS

Classical MD simulations for tantala were carried out using LAMMPS software [40]. Tantala is modeled via a modified van Beest, Kramer, and van Santen (BKS) potential [41] with an additional pseudo-covalent Morse term [42]. To speed up computations, we implemented Wolf truncation with a cut-off as proposed in Ref. 36. Each simulation consists of 2520 atoms, contained in a cubic box with periodic boundary conditions.

Atomic configurations were obtained with the following protocol. Tantala crystal is first equilibrated at 300 K and then rapidly heated to 5000 K. The liquid at 5000 K is equilibrated for 50 ns and then cooled down to 3000 K in the NPT ensemble ($P = 0$) with a cooling rate $q_f = 10^2$ K/ns. Final cooling from 3000 K to 300 K is achieved with a slower cooling rate $q_s = 10$ K/ns. With this recipe we generated 50 independent samples. All structural analysis were performed after the configurations were relaxed by energy minimization. We note that the faster quench rate $q_f = 10^2$ K/ns considered here is comparable to the slowest rate considered in previous works on tantala [36, 42].

III. RESULTS AND DISCUSSION

For a cooling rate $q_s = 10$ K/ns the great majority of the liquid samples, 45 over 50, experience crystallization, as signaled by the occurrence of a sharp change in the specific volume $\rho^{-1}(T)$ and visual inspection (not shown). In only 5 samples the solidification takes place in an amorphous state. We label the latter states as s1-s5. Their specific volume $\rho^{-1}(T)$ is plotted in Fig.1(a) in the whole temperature range under study.

The average density in the amorphous state at 300 K of the samples s1-s5 is 7.64 g/cm^3, i.e. well in the experimental range 7.30-7.68 g/cm^3 [43–45], whereas the liquid tantala at 2000 K exhibits a density of 7.27 g/cm^3 to be compared with the estimate 7.20 g/cm^3 [37].

The temperature where the glass transition (GT) takes place depends on the cooling rate and is conveniently defined by the temperature where the thermal expansion coefficient changes abruptly but continuously from the liquid to the glass value upon cooling [46]. We define $T_{g,n}$ as the GT temperature corresponding to the cooling rate $q_n = 10^n$ K/ns. In order to understand where GT is located at the cooling rate of our study $q_s = q_1$, we resort to previous studies showing that cooling the liquid at higher quench rates than q_s, i.e. q_2 and q_3, prevents the crystallization and leads to the

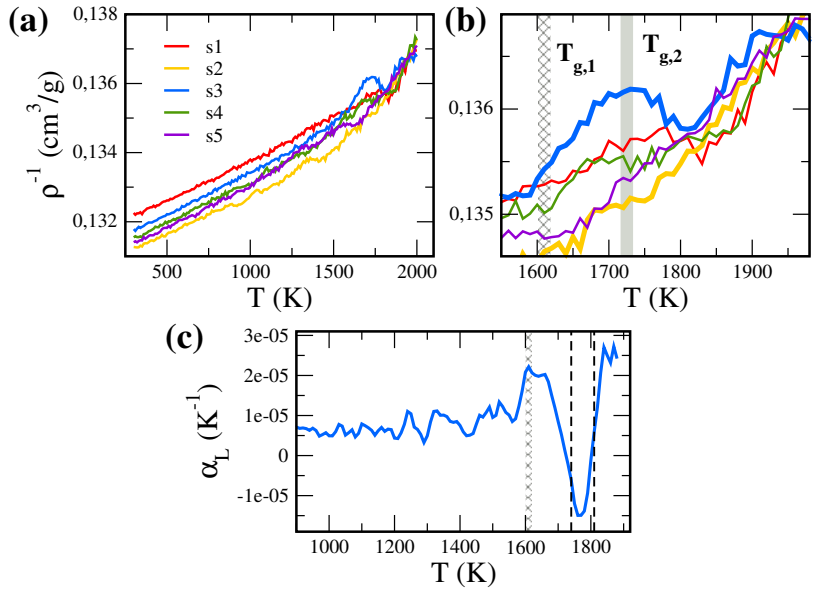

FIG. 1: Panel a): Temperature dependence of the inverse density ρ^{-1} for five samples, labelled s1-s5, during the quench from the liquid state with a rate 10 K/ns (full lines). Panel b): Magnification of the anomalous region. Samples s2 and s3, exhibiting the missing and the larger density anomalies respectively, are highlighted. The vertical shaded regions mark the estimated glass transition at the cooling rates 10 K/ns ($T_{g,1}$) and 10^2 K/ns ($T_{g,2}$), see text for details. Panel c): coefficient of linear thermal expansion of sample s3. The vertical dashed lines mark the NTE region. The minimum value is -14 ppm K^{-1}.

GT temperatures $T_{g,2} = 1725$ K and $T_{g,3} = 1820$ K, respectively [47]. Building on the fact that $d \log |q|/dT_g$ is nearly constant [48], one finds $T_{g,1} = 1610$ K. Henceforth, we limit our analysis to $T > T_{g,1}$. Further support to our choice about $T_{g,1}$ will be provided later.

No density anomaly was observed by cooling the liquid tantala at q_2 and q_3 [47]. Instead, for a cooling rate $q_s = q_1$ a NTE region is observed in three samples, s1, s3 and s4, see Figure 1(b). The coefficient of linear thermal expansion of sample s3 is shown in Figure 1(c).

Samples s2, s5 do not show NTE and solidify in the amorphous state around $T_{g,1}$. The density minimum is observed at a temperature which is *larger* than $T_{g,1}$, suggesting that both the density extrema and the whole NTE region are in the *liquid* regime. This conclusion may be made sounder and less dependent on the estimate $T_{g,1}$ by noting that the density minimum is close to $T_{g,2} = 1725$ K, i.e. the GT temperature corresponding to a one-order-of magnitude *faster* cooling rate. The fact that the density minimum is in the metastable liquid rules out that it is an artefact due to the intersection of the NTE region with GT and the subsequent recovery of the usual positive

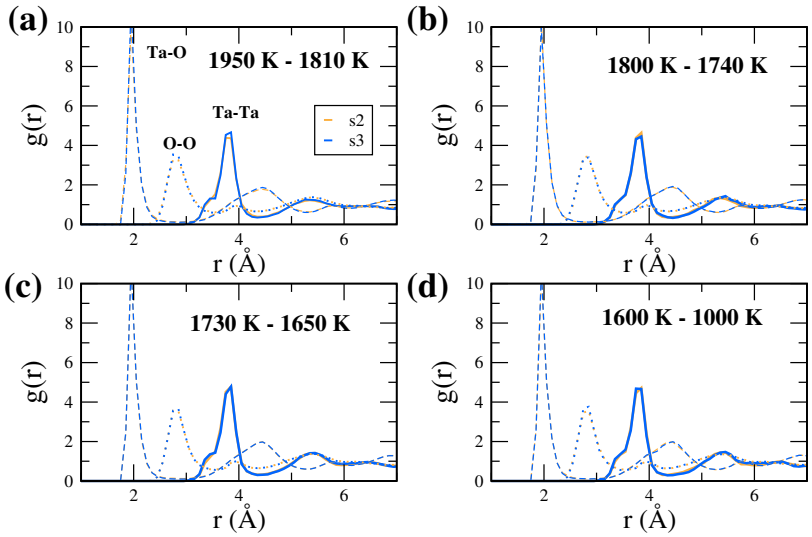

FIG. 2: Partial pair distribution functions of the samples s2 and s3, showing no anomaly and the strongest density anomaly, respectively. The panels refer to the following temperature ranges: (a) liquid, (b) NTE region, (c) the end of the NTE region down to GT, (d) amorphous state.

thermal expansivity by the glass.

The magnitude of the density anomaly depends on the sample under consideration. We interpret the finding in terms of sample-dependent, incomplete structural equilibration of the liquid due to the proximity of GT and NTE regions with the adopted cooling rate q_s. Indeed, the latter is a choice of compromise. The Tantala liquid, due to the strong tendency to crystallize, does not allow slower cooling rates to gain full equilibration of the NTE region. On the other hand, q_s is slow enough to distance GT from NTE and ensures sufficient suppression of off-equilibrium effects, which, if enhanced by rising the cooling rate at q_2 and then making GT and NTE closer to each other, would completely hide the density anomaly [47].

To gain more insight into the microscopic origin of the density anomaly of Tantala, we investigated the partial pair distribution functions $g_{i,j}$. They are plotted in Fig.2 for the samples with no (s2) or strongest (s3) density anomaly. The pattern depends weakly on the temperature in the investigated range. Considering the whole set of distribution functions, it was noted that both $g_{Ta,Ta}$ and $g_{O,O}$ exhibit clearer changes in amorphous and liquid tantala [37]. This offers a way to assess whether our system, during cooling, settled in a solid-like structure or persisted in a liquid-like one. In particular, $g_{Ta,Ta}$ shows that samples s2 and s3 exhibit nearly the same split of Ta-Ta nearest-neighbor peak which is more strikingly seen at 3.312(2) Å and 3.750(1) Å

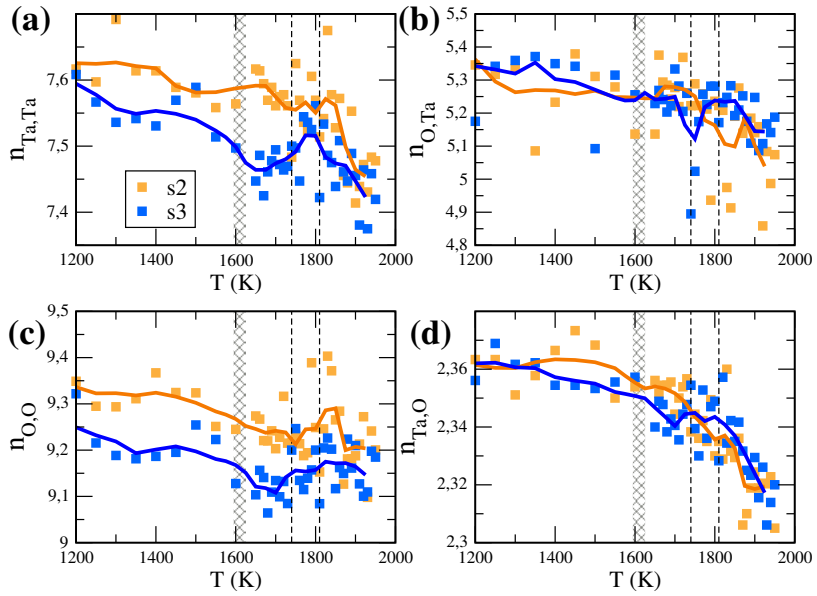

FIG. 3: Symbols: evolution of the partial coordination number for tantalum (panel a and b) and oxygen atoms (panel c and d) upon cooling, for the samples s2 and s3, showing none and strongest density anomaly, respectively. Lines are the running average of data in a temperature window corresponding to $50\,K$. The vertical dashed lines mark the NTE region of the s3 sample. The vertical shaded region marks the estimated glass transition $T_{g,1}$.

by experiments in ion-beam sputtered (IBS) tantala but *not* in liquid tantala [37]. Furthermore, inspection of $g_{O,O}$ shows that the O-O nearest-neighbor peak, which is drastically depressed in liquid Tantala, is rather close to the one of IBS tantala in both s2 and s3 samples [37]. The above analysis suggests a more solid-like structure of our samples in the investigated temperature range.

The experimental finding that $g_{Ta,Ta}$ and $g_{O,O}$ exhibit larger changes from the liquid to the solid state [37] suggests that they are efficient probes of the structural changes and may help to ascertain the microscopic nature of the density anomaly. Since the changes are anticipated to be tiny, given the poor temperature dependence of the partial pair distribution functions (Fig.2), we resort to the partial coordination numbers providing the integrated, overall modification of the first shell. Ref. [49] mentions the role of the partial coordination numbers in marking the NTE region of liquid As2Te2, providing additional motivations to this choice.

The results for the samples with no (s2) or strongest (s3) density anomaly are given in Fig.3, in terms of the average number of first-neighbor i atoms to a given j atom, $n_{i,j}$ with the first-neighbor pairs defined using the first minimum of the corresponding pair distribution function. It is seen that

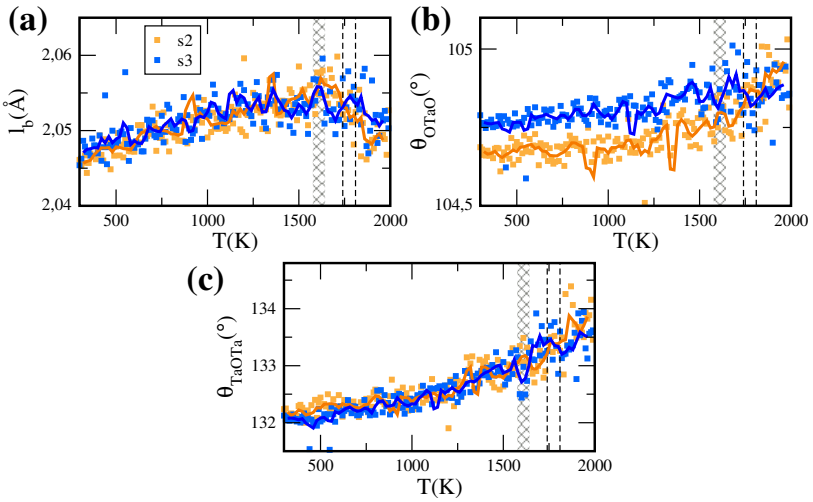

FIG. 4: Symbols: evolution of the O-Ta-O bond angle (panel a), Ta-O-Ta bond angle (panel b) and Ta-O bond length (panel c) upon cooling (samples s2 and s3). Lines are the running average of data in temperature window corresponding to $50\,K$. The vertical dashed lines highlight the NTE region of the s3 sample. The vertical shaded region marks the estimated glass transition $T_{g,1}$.

all the corresponding partial coordination numbers of the samples s2 and s3 are rather close in the highly mobile states at the highest temperature, suggesting structural similarity. On cooling, both $n_{Ta,O}$ and $n_{O,Ta}$ increase more or less in a continuous way and differ little in samples s2 and s3. Differently, subtle but appreciable non-monotonous changes are signaled by both $n_{Ta,Ta}$ and $n_{O,O}$ on approaching GT at $T_{g,1}$ from above. The changes are less perceived in the s2 sample, whereas they are clear in s3 with onset in the temperature range of the NTE region. As a result, both $n_{Ta,Ta}$ and $n_{O,O}$ are *smaller* in the amorphous state of s3 than in the s2 one. This offset is largely due to the fact that, leaving the NTE region on cooling but still *above* $T_{g,1}$, both $n_{O,O}$ and $n_{Ta,Ta}$ of the s3 sample *decrease*. The decrease of the coordination number on cooling across the NTE region, has been also reported for both Te [38, 39] and Ge [29]. On cooling further, the decrease is halted at GT and replaced in the amorphous state by a new regime of monotonous increase, as for all the other partial coordination numbers of both samples. It appears that, differently from the sample s2, the sample s3 was able to complete local rearrangements *above* GT, ensuring both a better equilibration and the emergence of the NTE region. This aspect will be scrutinised more in depth below with the analysis of other indicators.

Fig. 4 provides information about the temperature dependence of the geometry of the Ta-O

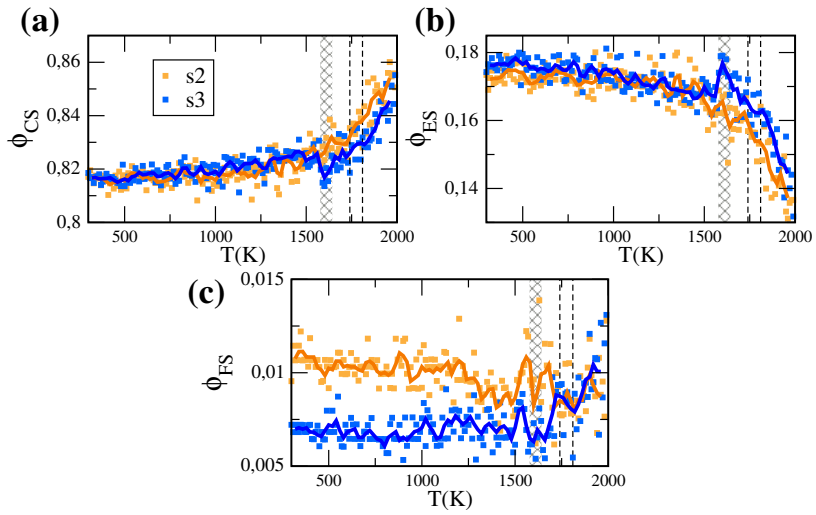

FIG. 5: Symbols: evolution of the fractions of corner sharing CS (panel a), edge sharing ES (panel b) and face sharing FS (panel c) polyhedra upon cooling (samples s2 and s3). Lines are the running average of data in temperature window corresponding to $50\,K$. The vertical dashed lines highlight the NTE region of the s3 sample. The vertical shaded region marks the estimated glass transition $T_{g,1}$.

bond network, namely the O-Ta-O bond angle (panel a), the Ta-O-Ta bond angle (panel b) and Ta-O bond length (panel c) of the samples s2 and s3. The latter two parameters are found to be nearly coincident in the two samples. In particular, the Ta-O-Ta bond angle decreases continuously with the temperature, whereas the Ta-O bond length has a rounded maximum at about GT. The O-Ta-O bond angle (Fig.4a) of the s2 sample becomes slightly less than the one of the s3 one, roughly below the NTE region. Given the extremely small differences of the geometry of the Ta-O bond network in samples s2 and s3 shown in Fig.4, it is difficult to draw sound conclusions about their role in the microscopic origin of the density anomaly.

Fig.5 provides the results of the analysis of the tantala structure at different temperatures in terms of polyhedra of the samples s2 and s3. The fraction of corner sharing ϕ_{CS}, Fig.5(a), and edge sharing ϕ_{ES}, Fig.5 (b), is quite close in the two samples (small differences in the liquid state above GT are ascribed to the difficulty of the analysis when the polyhedra are rather distorted by thermal effects and their statistical distribution is wider than in the solid state [50]). A tendency to have more compact structures is signalled by both the decrease of ϕ_{CS} and the increase of ϕ_{ES} by lowering the temperature. The latter has been evidenced by neutron and X-ray scattering experiments [37]. Fig.5 (c) plots the fraction of face sharing ϕ_{FS} which is rather small. Interestingly,

ϕ_{FS} of the sample s3 tends to decrease by lowering the temperature and freezes *below GT*. Distinctly, the sample s2 freezes ϕ_{FS} *above* GT. This behaviour parallels the temperature dependence of the partial coordination numbers $n_{Ta,Ta}$ and $n_{O,O}$ of the samples s2 and s3, see Fig.3(a) and Fig.3(b), respectively. It is tempting to conclude that the equilibration process of the sample s2 was incomplete, thus preventing the emergence of the NTE region.

A comparison of the present results with other NTE materials is worthwhile. Stable water has $\alpha_L = -23$ ppm K^{-1} at 273 K and exhibits, together with other thermodynamic properties, a well-known singularity in the supercooled regime at about 227 K [51, 52]. In more detail, Table I compares the characteristics of the NTE region of Ta_2O_5 with other systems, reporting, in addition to the linear thermal expansion α_L, also the NTE range ΔT and the relative volume change $\Delta V/V$. The table combines simulation data on SiO_2 [28] and Ge [29], with experimental data on liquid Te [22] and solid-state materials reviewed in ref. [14].

TABLE I: Comparison between in-silico Ta_2O_5 , SiO_2 and Ge , and experimental data on liquid Te and representative solid-state systems with giant isotropic NTE.

Materials	T_{NTE} (K)	ΔT (K)	α_L (ppm K^{-1})	$\Delta V/V$ (%)	Category [a]	State	Ref.
in silico Ta_2 O_5	$1725-1825$	100	-14	0.42	CV	liquid	PW
in silico SiO_2	$3400-4400$	1000	-9	2.7	CV	liquid	[28]
in silico Ge	$1500-2400$	900	-40	8	CV	liquid	[29]
Te	$550-740$	190	-150	8.5	CV	liquid	[22]
ZrW_2O_8	2–1443	1441	$-6 \sim -9$	2.7	CV	solid	[14]
$Cd(CN)_2{\cdot}xCCl_4$	170–375	205	-34	2.1	CV	solid	[14]
$Mn_3Ga_{0.7}Ge_{0.3}N_{0.88}C_{0.12}$	197–319	122	-18	0.5	MG	solid	[14]
$LaFe_{10.5}Co_{1.0}Si_{1.5}$	240–350	110	-26	1.1	MG	solid	[14]
$SrCu_33Fe_4O_{12}$	180–250	70	-20	0.4	CT	solid	[14]

[a] CV, conventional; MG, magnetic transition; CT, charge-transfer transition

IV. CONCLUSIONS

We revealed the presence of density anomaly in supercooled tantala. The sample preparation needed to highlight this phenomena is critical, due to two contrasting requirements, i.e. the need to cool the liquid slowly in order to suppress non-equilibrium effects masking the anomaly on one side and, on the other, to avoid crystallization as promoted by slower cooling. The resulting set showing NTE was analyzed using different structural indicators. The density anomaly is found to be best signalled by the decrease of the partial coordination numbers $n_{Ta,Ta}$ and $n_{O,O}$ while temperature decreases.

Acknowledgments

This project has received funding from the European Union's Horizon 2020 research and innovation programme under the Marie Sklodowska-Curie grant agreement No 754496. A generous grant of computing time from Green Data Center of the University of Pisa and Dell® Italia is gratefully acknowledged.

[1] D. S. Eisenberg and W. Kauzmann, *The structure and properties of water* (Oxford University Press, Oxford, 2005).

[2] P. G. Debenedetti, Journal of Physics: Condensed Matter **15**, R1669 (2003).

[3] C. A. Angell and H. Kanno, Science **193**, 1121 (1976), ISSN 0036-8075, https://science.sciencemag.org/content/193/4258/1121.full.pdf.

[4] R. Brückner, Journal of Non-Crystalline Solids **5**, 123 (1970), ISSN 0022-3093.

[5] Y. I. Sharykin, V. P. Glazkov, S. N. Skovorod'ko, V. A. Somenkov, V. A. Fomin, S. S. Shilshtein, and E. E. Shpil'rain, Dokl. Akad. Nauk SSSR **244**, 78 (1979).

[6] S. J. Kennedy and J. C. Wheeler, The Journal of Chemical Physics **78**, 1523 (1983), https://doi.org/10.1063/1.444842.

[7] H. Thurn and J. Ruska, Journal of Non-Crystalline Solids **22**, 331 (1976).

[8] Y. Tsuchiya, Journal of the Physical Society of Japan **60**, 227 (1991), https://doi.org/10.1143/JPSJ.60.227.

[9] C. Bichara, M. Johnson, and J. Y. Raty, Phys. Rev. Lett. **95**, 267801 (2005).

[10] C. A. Angell, R. D. Bressel, M. Hemmati, E. J. Sare, and J. C. Tucker, Phys. Chem. Chem. Phys. **2**, 1559 (2000).

[11] T. A. Mary, J. S. O. Evans, T. Vogt, and A. W. Sleight, Science **272**, 90 (1996), ISSN 0036-8075, https://science.sciencemag.org/content/272/5258/90.full.pdf.

[12] C. Lind, Materials **5**, 1125 (2012), ISSN 1996-1944.

[13] M. T. Dove and H. Fang, Reports on Progress in Physics **79**, 066503 (2016).

[14] K. Takenaka, Frontiers in Chemistry **6**, 267 (2018), ISSN 2296-2646.

[15] C. Romao, K. Miller, C. Whitman, M. White, and B. Marinkovic, in *Comprehensive Inorganic Chemistry II (Second Edition)*, edited by J. Reedijk and K. Poeppelmeier (Elsevier, Amsterdam, 2013), pp. 127–151, second edition ed., ISBN 978-0-08-096529-1.

[16] C. Otjacques, J.-Y. Raty, M.-V. Coulet, M. Johnson, H. Schober, C. Bichara, and J.-P. Gaspard, Phys. Rev. Lett. **103**, 245901 (2009).

[17] P. Kumar, S. V. Buldyrev, F. Sciortino, E. Zaccarelli, and H. E. Stanley, Phys. Rev. E **72**, 021501 (2005).

[18] L. Xu, S. V. Buldyrev, N. Giovambattista, C. A. Angell, and H. E. Stanley, The Journal of Chemical Physics **130**, 054505 (2009), https://doi.org/10.1063/1.3043665.

[19] H. Kanno, H. Yokoyama, and Y. Yoshimura, The Journal of Physical Chemistry B **105**, 2019 (2001).

[20] P. G. Debenedetti and M. C. D'Antonio, The Journal of Chemical Physics **84**, 3339 (1986), https://doi.org/10.1063/1.450269.

[21] P. G. Debenedetti and M. C. D'Antonio, AIChE Journal **34**, 447 (1988), https://aiche.onlinelibrary.wiley.com/doi/pdf/10.1002/aic.690340312.

[22] Y. Tsuchiya, Journal of Physics: Condensed Matter **3**, 3163 (1991).

[23] Y. Tver'yanovich, V. Ushakov, and A. Tverjanovich, Journal of Non-Crystalline Solids **197**, 235 (1996), ISSN 0022-3093.

[24] J. Ruska and H. Thurn, Journal of Non-Crystalline Solids **22**, 277 (1976).

[25] D. Liu, Y. Zhang, C.-C. Chen, C.-Y. Mou, P. H. Poole, and S.-H. Chen, Proceedings of the National Academy of Sciences **104**, 9570 (2007), ISSN 0027-8424, https://www.pnas.org/content/104/23/9570.full.pdf.

[26] F. Mallamace, C. Branca, M. Broccio, C. Corsaro, C.-Y. Mou, and S.-H. Chen, Proceedings of the National Academy of Sciences **104**, 18387 (2007), ISSN 0027-8424, https://www.pnas.org/content/104/47/18387.full.pdf.

[27] S. Sen, R. L. Andrus, D. E. Baker, and M. T. Murtagh, Phys. Rev. Lett. **93**, 125902 (2004).

[28] J. Luo, Y. Zhou, C. G. Pantano, and S. H. Kim, Journal of the American Ceramic Society **101**, 5419 (2018).

[29] J. K. Bording, Phys. Rev. B **62**, 7103 (2000).

[30] C. Angell, C. Moynihan, and M. Hemmati, Journal of Non-Crystalline Solids **274**, 319 (2000), ISSN 0022-3093, physics of Non-Crystalline Solids 9.

[31] M. Hemmati, C. T. Moynihan, and C. A. Angell, The Journal of Chemical Physics **115**, 6663 (2001), https://doi.org/10.1063/1.1396679.

[32] P. H. Poole, I. Saika-Voivod, and F. Sciortino, Journal of Physics: Condensed Matter **17**, L431 (2005).

[33] D. Paschek, Phys. Rev. Lett. **94**, 217802 (2005).

[34] V. V. Brazhkin and A. G. Lyapin, Journal of Physics: Condensed Matter **15**, 6059 (2003).

[35] J. P. Trinastic, R. Hamdan, C. Billman, and H.-P. Cheng, Phys. Rev. B **93**, 014105 (2016).

[36] T. Damart, E. Coillet, A. Tanguy, and D. Rodney, J. Appl. Phys. **119**, 175106 (2016).

[37] O. L. G. Alderman, C. J. Benmore, J. Neuefeind, E. Coillet, A. Mermet, V. Martinez, A. Tamalonis, and R. Weber, Phys. Rev. Materials **2**, 043602 (2018).

[38] T. Tsuzuki, M. Yao, and H. Endo, Journal of the Physical Society of Japan **64**, 485 (1995), https://doi.org/10.1143/JPSJ.64.485.

[39] G. Zhao and Y. N. Wu, Phys. Rev. B **79**, 184203 (2009).

[40] S. Plimpton, J. Comput. Phys. **117**, 1 (1995).

[41] B. W. H. van Beest, G. J. Kramer, and R. A. van Santen, Phys. Rev. Lett. **64**, 1955 (1990).

[42] J. P. Trinastic, R. Hamdan, Y. Wu, L. Zhang, and H.-P. Cheng, J. Chem. Phys. **139**, 154506 (2013).

[43] N. Banno, T. Sakamoto, N. Iguchi, M. Matsumoto, H. Imai, T. Ichihashi, S. Fujieda, K. Tanaka, S. Watanabe, S. Yamaguchi, et al., Applied Physics Letters **97**, 113507 (2010), https://doi.org/10.1063/1.3488830.

[44] R. Bassiri, K. B. Borisenko, D. J. H. Cockayne, J. Hough, I. MacLaren, and S. Rowan, Applied Physics Letters **98**, 031904 (2011), https://doi.org/10.1063/1.3535982.

[45] T. Li, F. A. Aguilar Sandoval, M. Geitner, L. Bellon, G. Cagnoli, J. Degallaix, V. Dolique, R. Flaminio, D. Forest, M. Granata, et al., Phys. Rev. D **89**, 092004 (2014).

[46] P. G. Debenedetti and F. H. Stillinger, Nature **410**, 259 (2001).

[47] F. Puosi, F. Fidecaro, S. Capaccioli, D. Pisignano, and D. Leporini, Phys. Rev. Research **1**, 033121 (2019).

[48] C. T. Moynihan, A. J. Easteal, J. Wilder, and J. Tucker, The Journal of Physical Chemistry **78**, 2673 (1974).

[49] C. Otjacques, J.-Y. Raty, F. Hippert, H. Schober, M. Johnson, R. Céolin, and J.-P. Gaspard, Phys. Rev. B **82**, 054202 (2010).

[50] J. C. G. Montoro and J. L. F. Abascal, The Journal of Physical Chemistry **97**, 4211 (1993).

[51] R. J. Speedy, The Journal of Physical Chemistry **91**, 3354 (1987).

[52] H. Sippola and P. Taskinen, Journal of Chemical & Engineering Data **63**, 2986 (2018), https://doi.org/10.1021/acs.jced.8b00251.